

# Studies of the aperture design and its pointing precision in fast neutron penumbral imaging<sup>\*</sup>

LIU Dong-Jian(刘东剑)<sup>1,2</sup> AN Zhu(安竹)<sup>1;1)</sup> TANG Chang-Huan(唐昶环)<sup>2</sup> ZOU Lian(邹炼)<sup>1</sup>

<sup>1</sup> (Institute of Nuclear Science and Technology, Key Laboratory for Radiation Physics and Technology of Education Ministry, Sichuan University, Chengdu 610064, China)

<sup>2</sup> (Laser Fusion Research Center, China Academy of Engineering Physics, Mianyang 621900, China)

**Abstract** Neutron penumbral imaging technique is an important diagnosis method in Inertial Confined Fusion, and the design of the aperture shape will affect the resolution of the imaging system. In this paper, several designs of the aperture shape are discussed. Moreover, the pointing precision is also discussed, and a rational pointing precision is given.

**Key words** inertial confined fusion, neutron penumbral imaging, classical molecular dynamics method

**PACS** 52.57.-z, 42.30.Wb, 02.70.Ns

## 1 Introduction

As the size of ICF target increases, the absorption of X radiation emitting from a burning target increases as well. Therefore, we can not use the X-ray diagnosis to observe the burning target. As one of the fusion productions, fast neutrons have high penetrating capability, so they can be used to diagnosis the burning of the target<sup>[1]</sup>. We will review the principle of penumbral imaging first, and then we will discuss the effect of aperture shape design and pointing error to the imaging

## 2 Fast neutron penumbral imaging

### 2.1 The principle of imaging

The principle of fast neutron penumbral imaging is shown in Fig. 1. The fast neutrons emitting from a burning target are scattered by the aperture materials, and form an penumbral image on the detector arrays<sup>[2, 3]</sup>.

The apertures are made by heavy metal materials, such as Au or Pb, so neutrons are always scattered into large solid angles. But the solid angle of a detector is small, so only the neutrons without scattering pass the aperture and few scattered neutrons can

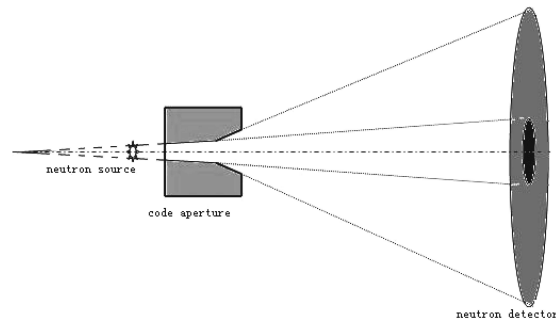


Fig. 1. Principle of penumbral imaging.

reach the detector arrays. These neutrons collide with the detector's materials, deposit energies and then are recorded by the detector. The encoded image consists of a uniformly bright region surrounded by a penumbral region. Considering a neutron source with the intensity distribution  $O(r)$  illuminating a neutron

Received 8 July 2008

<sup>\*</sup> Supported by National Natural Science Foundation of China (10535030) and Program for New Century Excellent Talents in University (NCET-05-0780)

1) E-mail: anzhu@scu.edu.cn

detector through aperture  $h(r, r')$  (i.e., PSFs), the penumbra  $i(r)$  on the imaging plane can be described by the following equation:

$$i(r) = \int h(r; r') \cdot O(r') dr'. \quad (1)$$

If we know  $h(r, r')$  in advance, we can obtain the intensity distribution  $O(r)$  of the neutron source by some deconvolution methods.

## 2.2 Reconstruction of the penumbral imaging

In penumbral imaging, original shapes of the neutron sources can be reconstructed from the detected penumbral images. There are many reconstruction methods, which we can assort into two categories, namely, linear methods and nonlinear methods. In penumbral imaging, linear reconstruction methods are often adopted by some research groups. However, these linear methods have some shortcomings. One of these shortcomings is the aberration<sup>[4]</sup> in their results, because they presume that point spread functions (PSF) are isoplanatic (space-invariant), and this presumption is only approximately valid. Therefore, we have developed a new nonlinear reconstruction method based on classical molecular dynamics (CMD)<sup>[5-7]</sup>, which can overcome the disadvantages of linear methods by using space-variant PSFs.

By using the CMD method, firstly we chose one object function as<sup>[7]</sup>:

$$O(\mathbf{I}, \mathbf{P}) = \sum_X^{N_X} \sum_Y^{N_Y} \left[ \sum_x^{n_x} \sum_y^{n_y} I(x, y) P(X, Y; \{x, y\}) - \overline{P}(X, Y) \right]^2. \quad (2)$$

where  $I(x, y)$  is the intensity of neutron source resolution unit at the point  $(x, y)$  on source plane,  $P(X, Y; \{x, y\})$  is the contribution of point source  $I(x, y)$  to the detector unit at the point  $(X, Y)$  on imaging plane (i.e., PSF), and  $\overline{P}(X, Y)$  is the detected image.  $N_X$  and  $N_Y$  are the maximum detector unit numbers on  $x$  and  $y$  axes on the imaging plane.  $n_x$  and  $n_y$  are maximum resolution unit numbers on  $x$  and  $y$  axes on the source plane. By introducing the concepts of virtual atom and virtual cluster, the reconstruction process can be considered as an analogy to finding the equilibrium configuration of a virtual cluster. Then, we can make an analogy between

$O(\mathbf{I}, \mathbf{P})$  to potential  $V(\mathbf{r}_i)$ :

$$V(\mathbf{r}_i) = O(\mathbf{I}, \mathbf{P}). \quad (3)$$

When the system relaxes to an equilibrium state, it has the lowest free energy, and the optimization source intensity distribution is obtained. The dynamics equation for the virtual cluster system can be written as:

$$M_i \frac{d^2 I_i}{d\tau^2} = - \frac{\partial O(\mathbf{I}, \mathbf{P})}{\partial I_i}, \quad (4)$$

$$M_i = \sum_{x_j}^{n_x} \sum_{y_j}^{n_y} \sum_X^{N_X} \sum_Y^{N_Y} P(X, Y; \{x_i, y_i\}) P(X, Y; \{x_j, y_j\}), \quad (5)$$

where  $I$  is the neutron intensity distribution,  $I_i$  is the  $i$ th element of  $I$ ,  $\tau$  is the virtual time, and  $M_i$  is the mass of the atom defined according to the objective function adopted. We can solve Eq. (4) by various finite differential approaches. Here we use the following method: the force on atom  $j$  is

$$f_j = - \frac{\partial O(\mathbf{I}, \mathbf{P})}{\partial I_j} = \sum_{i \neq j}^{n_x \times n_y} f_{ij} - I_j \sum_{i=1}^{n_x \times n_y} D_{ij} + \sum_{i=1}^{n_x \times n_y} \overline{D}_{ij}, \quad (6)$$

where

$$f_{ij} = (I_j - I_i) D_{ij},$$

$$D_{ij} = \sum_X^{N_X} \sum_Y^{N_Y} P(X, Y; \{x_i, y_i\}) P(X, Y; \{x_j, y_j\}),$$

$$\overline{P}(X, Y; \{x_i, y_i\}) =$$

$$P(X, Y; \{x_i, y_i\}) \overline{P}(X, Y) / \sum_X^{N_X} \sum_Y^{N_Y} P(X, Y; \{x_i, y_i\}).$$

By solving the Eq. (6), we can obtain the optimal neutron source distribution<sup>[5, 7]</sup>.

## 3 Discussion of the aperture shape design and pointing error

### 3.1 Discussion of aperture shape design

The layout of experiment is shown in Fig. 2. All the penumbral images used below are simulated by using Monte Carlo method. And the material of apertures is Au.

The shape design of aperture is very important in penumbral imaging technique. For the strong penetration ability of fast neutrons, the materials of apertures are often heavy metals, such as Au, Pb and W. In order to obtain a high resolution, the shapes of the apertures should be optimized to get penumbral images with enough contrast grade and be sensitive to the source intensity distribution, and the spread of

the PSF should be small enough as well<sup>[8]</sup>. Bicone, straight hole and ring hole apertures are often used<sup>[9]</sup>. We will compare them in the followings.

Figure 3 gives the PSFs and PSF spreads of the four shape designs, and we can see that the PSF spreads of the bicone and the bicone aperture with bicone plug are smaller. When the neutron yield is low, the bicone shape would be better, because its hole has a larger solid angle. So in general the bicone shape is the most suitable one in the four shape

designs.

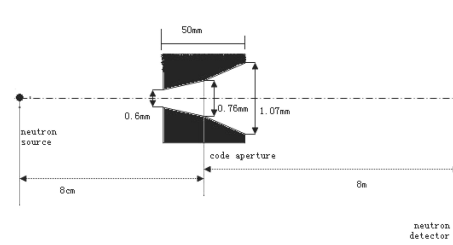


Fig. 2. Layout of penumbral imaging.

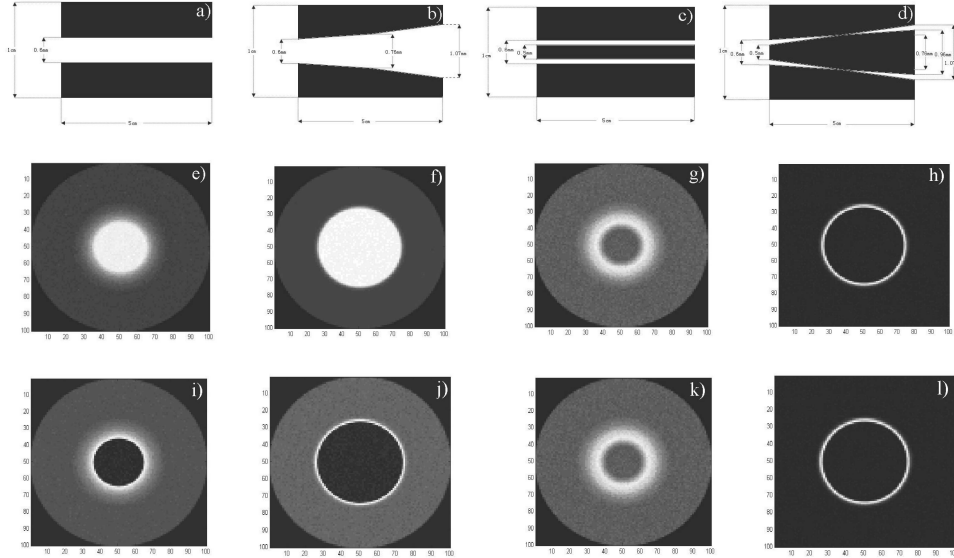


Fig. 3. Four shape designs of aperture. a) straight hole; b) bicone; c) ring hole; d) bicone hole with bicone plug; e) PSF of straight hole; f) PSF of bicone; g) PSF of ring hole; h) PSF of bicone hole with bicone plug; i) PSF spread of straight hole; j) PSF spread of bicone; k) PSF spread of ring hole; l) PSF spread of bicone hole with bicone plug.

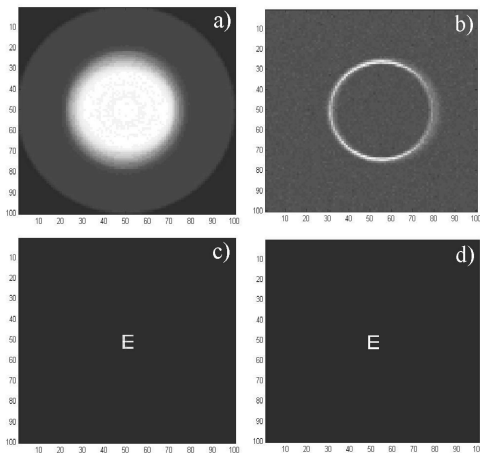


Fig. 4. Some reconstructions of 'E' shape source by CMD method. a) penumbral image of 'E' shape source through bicone aperture; b) penumbral image of 'E' shape source through bicone aperture with bicone plug; c) CMD reconstruction of a); d) CMD reconstruction of b).

Figure 4 shows the reconstructions of penumbral images through the bicone aperture and the bicone aperture with bicone plug. We can see that the bicone aperture with bicone plug can achieve higher resolution. Therefore, when the neutron yield is large enough, the bicone aperture with bicone plug can be used.

### 3.2 Discussion of the pointing error

Ideally, the aperture axis and imaging axis should be at the same direction line. But in fact this can not be achieved exactly in experiments, and an angle between them is inevitably introduced. This angle will induce errors in reconstruction results. So the pointing error effects should be discussed.

By comparing the reconstruction results of penumbral images of the point source on imaging axis at different pointing errors with a reconstruction re-

sult without pointing error, we can get a maximum pointing error which can not be exceeded in the future experiment. Fig. 5 shows some results for a point neutron source and an ‘E’-shape neutron source with pointing error at the range from  $0.01^\circ$ — $0.5^\circ$ .

From Fig. 5, we can see that the reconstruction result of ‘E’ shape source is blurry when the pointing

error reaches  $0.5^\circ$ . For the point neutron sources, the intensity of the noise signal in the reconstruction result is about 1/2 of the real signal when the pointing error is  $0.05^\circ$ , and the real signal has been exceeded by the error signal when pointing error is  $0.1^\circ$ . So it can be concluded that the pointing error should not exceed  $0.05^\circ$ .

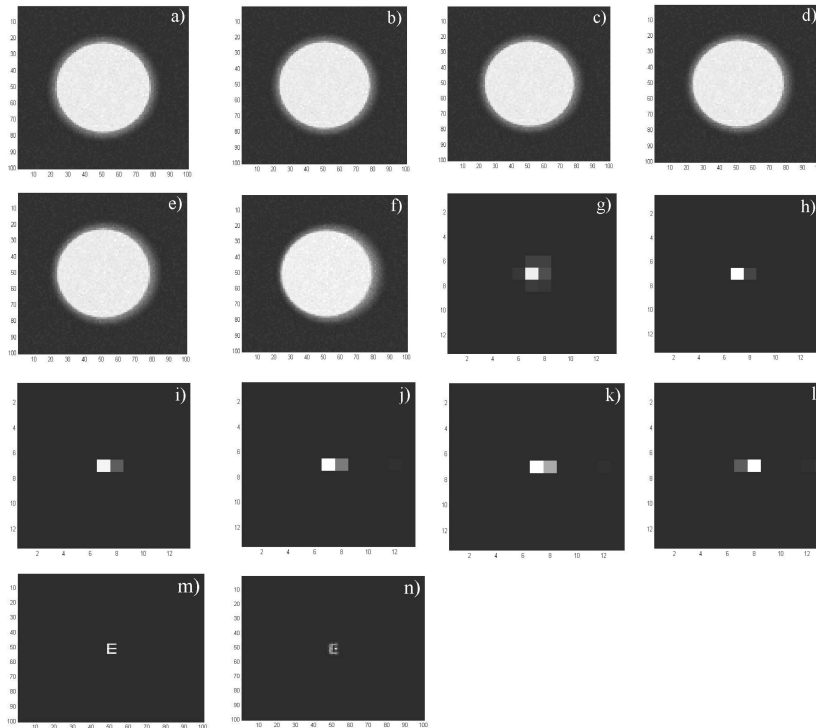


Fig. 5. Reconstruction results by the CMD method of penumbral images with different pointing errors. a) penumbral image with pointing error of  $0.01^\circ$ ; b) penumbral image with pointing error of  $0.02^\circ$ ; c) penumbral image with pointing error of  $0.03^\circ$ ; d) penumbral image with pointing error of  $0.04^\circ$ ; e) penumbral image with pointing error of  $0.05^\circ$ ; f) penumbral image with pointing error of  $0.1^\circ$ ; g) reconstruction result of a); h) reconstruction result of b); i) reconstruction result of c); j) reconstruction result of d); k) reconstruction result of e); l) reconstruction result of f); m) reconstruction result of ‘E’ shape neutron source without pointing error; n) reconstruction result of ‘E’ shape neutron source with pointing error of  $0.5^\circ$ .

## 4 Conclusions

From the discussion above, we can conclude that the shape of the ICF target can be reconstructed by fast neutron penumbral imaging method. When the

neutron flux is smaller the bicone aperture should be used in experiments due to its smaller PSF spread and larger solid angle, and when the neutron flux is larger, the bicone aperture with bicone plug can be used. The allowable maximum pointing error is  $0.05^\circ$ .

## References

- 1 Nugent K A. *Rev. Sci. Instrum.*, 1988, **59**(8): 1658—1663
- 2 Rouyer A. *Rev. Sci. Instrum.* 2003, **74**(3): 1234—1239
- 3 LIU Dong-Jian, TANG Chang-Huan, ZHAO Zong-Qing et al. *High Power Laser and Particle Beams*, 2006, **18**(7): 1199—11202
- 4 CHEN Y W, Nakao Z, Arakaki K et al. *IEEE Trans. Nucl. Sci.*, 1997, **NS-44**(3): 905—910
- 5 HOU Q, WANG Y. *Phys. Rev. Lett.*, 2001, **87**(16): 168101-1-3
- 6 HOU Q, WANG J, CHEN Y et al. *Med. Phys.*, 2003, **30**(1): 61—68
- 7 LIU DJ, ZOU L, TANG CH et al. *Nucl. Instrum. Methods Phys. Res. A*, 2007, **578**(3): 537—542
- 8 Disdier L, Rouyer A, Fedotoff A et al. *Rev. Sci. Instrum.*, 2003, **74**(3): 1832—1836
- 9 Barrera C A, Morse E C, Moran M J et al. *Rev. Sci. Instrum.*, 2006, **77**(10): 10E716-1-3